# Chronically implantable LED arrays for behavioral optogenetics in primates

Rishi Rajalingham[1,2], Michael Sorenson[3], Reza Azadi [4], Simon Bohn[4], James J. DiCarlo [1,2,3,5] and Arash Afraz [4✉]

Optogenetic methods have been widely used in rodent brains, but remain relatively under-developed for nonhuman primates such as rhesus macaques, an animal model with a large brain expressing sophisticated sensory, motor and cognitive behaviors. To address challenges in behavioral optogenetics in large brains, we developed Opto-Array, a chronically implantable array of light-emitting diodes for high-throughput optogenetic perturbation. We demonstrated that optogenetic silencing in the macaque primary visual cortex with the help of the Opto-Array results in reliable retinotopic visual deficits in a luminance discrimination task. We separately confirmed that Opto-Array illumination results in local neural silencing, and that behavioral effects are not due to tissue heating. These results demonstrate the effectiveness of the Opto-Array for behavioral optogenetic applications in large brains.

A key goal in systems neuroscience is to uncover the specific neural mechanisms that underlie behaviors of interest. Perturbation tools such as pharmacological, electrical and optogenetic stimulation and inhibition of neural activity have been critical to test the causal role of neural activity in different brain subregions in various behaviors. In particular, optogenetic perturbation, whereby light-sensitive ion channels and pumps[1,2] are embedded in the membrane of genetically targeted neurons to modulate their activity via delivery of light, has revolutionized neuroscience research by affording the ability to both drive and inhibit neural activity with precise temporal delimitation and cell-type specificity. Optogenetic tools may also offer promise for clinical applications, such as visual prosthetics and vision restoration[3].

Despite the widespread use of optogenetic methods in rodent brains, considerably fewer studies have shown behavioral effects of optogenetic perturbation in nonhuman primates (NHPs) despite substantial interest[4–11] (for example, 17 studies to date on rhesus macaque monkeys; Supplementary Table 1). The dearth of documented behavioral impacts using optogenetics in NHPs may stem from several problems, including difficulties of successful genetic targeting of neurons and of delivering sufficient light to perturb those neurons in the primate brain. A typical primate optogenetic experiment consists of first injecting a viral opsin acutely in the brain, either in a sterile surgery or through an implanted recording chamber. Following viral expression in the targeted cortical tissue, light from an external laser or light-emitting diode (LED) light source is delivered through an optical fiber acutely inserted into the brain, often coupled with a recording electrode[12].

There are two major problems with light delivery through an optical fiber. First, the acute nature of optical fiber experiments limits the number of experimental conditions and data trials, as the fiber cannot be returned to exactly the same position across multiple days. Second, given the size and shape of optical fibers, each penetration comes with a substantial cost of tissue damage and risk of hitting small arteries on the fiber path. This limits the number of practical fiber penetrations and thus constrains the number of variables, experimental conditions and trial counts that can be assessed in an animal. Moreover, the damage associated with fiber penetrations constrains the maximum diameter of the fiber, thus substantially limiting the cortical surface area that can be illuminated. This is a considerable limitation when working with large brains.

There have been several attempts to innovate on the optical fiber-based approach. First, by sharpening the tip of the fiber, it is possible to increase the cone of illumination while maintaining a small fiber diameter[13–15], but the gain in illumination volume is modest and the approach remains an acute protocol. Direct illumination of the cortex through transparent artificial dura has been used to bypass the problems associated with optical fibers[16–18]. This approach allows for a flexible illumination volume, mitigates tissue damage and could be used in a chronic manner. Furthermore, this approach can be coupled with red-shifted opsins to increase illumination depth[19]. However, direct illumination through artificial dura requires visual access via cranial windows, which is limited to brain subregions that permit direct optical access, and poses other challenges, including the risk of infection. Chronically implanted illumination devices could in principle address many of these problems[20,21], as they allow reliable targeting of the same cortical position across multiple days, and do not pose any safety issues related to tissue damage from acute probe insertions or infection from open chambers. However, given difficulties arising from the number of independently controlled illumination sources, none of the existing chronic illumination devices are currently capable of both large-scale and high-resolution illumination.

## Results

**Opto-Array specifications and properties.** To facilitate optogenetic experiments in NHPs, we have developed Opto-Array (Blackrock Microsystems), a chronically implantable array of LEDs. This tool harnesses the advantages of optogenetics—the precise spatial and temporal control of genetically specified neurons—but offers three additional advantages. First, the chronic nature of this tool enables stable experimental perturbation of the same neural population over

[1]Department of Brain and Cognitive Sciences, Massachusetts Institute of Technology, Cambridge, MA, USA. [2]McGovern Institute for Brain Research, Massachusetts Institute of Technology, Cambridge, MA, USA. [3]BlackRock Microsystems, Salt Lake City, UT, USA. [4]National Institute of Mental Health, NIH, Bethesda, MD, USA. [5]Center for Brains, Minds and Machines, Massachusetts Institute of Technology, Cambridge, MA, USA. ✉e-mail: arash.afraz@nih.gov
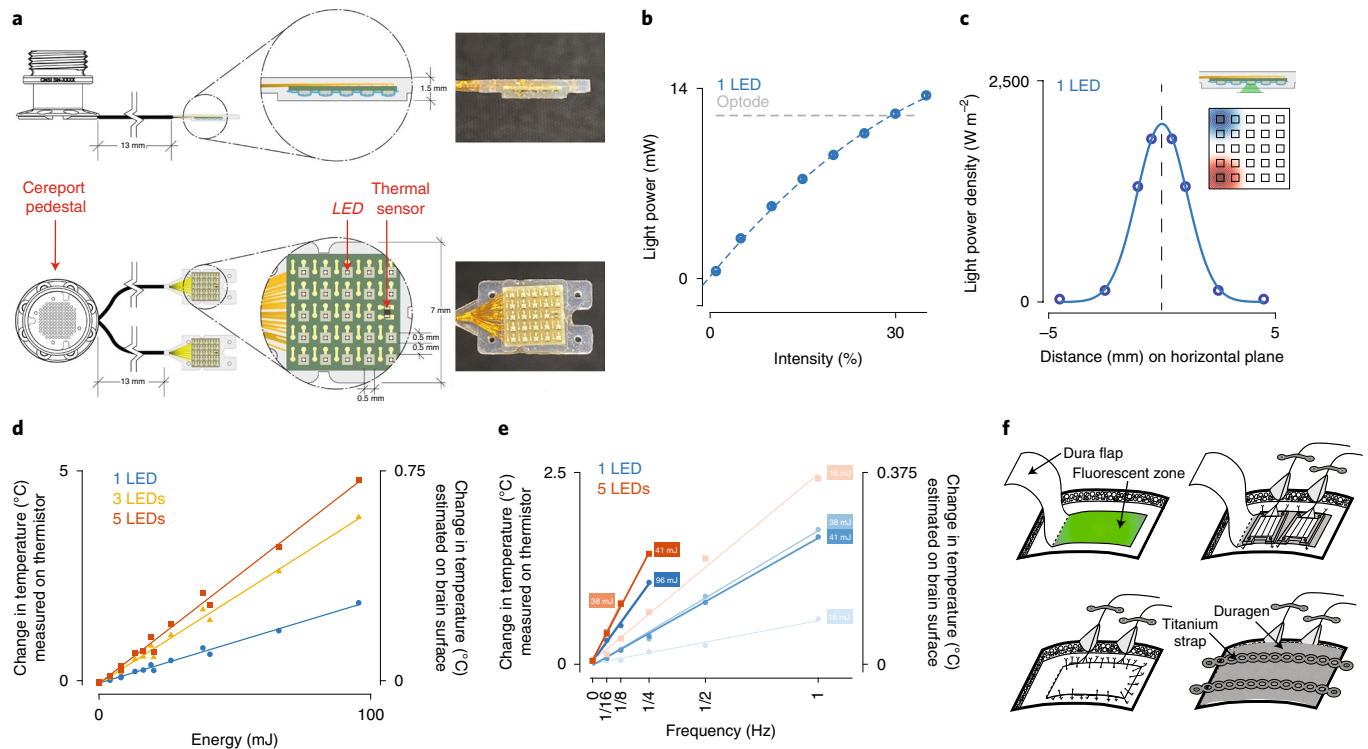
**Fig. 1 | Opto-Array design. a**, Schematic of the Opto-Array design. **b**, Light power output for individual LEDs as a function of the input intensity, controlled via input voltage (mean ± s.e.m. over repetitions; $n > 10$ repetitions for all intensity values). The horizontal dashed line corresponds to average power output of optrodes that have yielded measurable behavioral effects in monkeys. **c**, Spatial density of light power on the horizontal plane at a transverse distance of <1 mm from the surface of the LED. The spatial spread of light power over the horizontal plane is larger than the size of individual LEDs (full-width at half-maximum = 2.6 mm). The inset shows that activating more distant individual LEDs yields largely nonoverlapping light patterns on the cortical surface. **d**, Maximal increase in temperature (maximum across time, and average over repetitions) measured from an on-board thermal sensor, from activating different groups of LEDs as a function of the input energy (combining electrical power and illumination duration). The temperature increase measured by the on-board thermistor is shown on the left *y* axis, while the estimated temperature increase on the surface of the brain (based on a finite-element model; Extended Data Fig. 1) is shown on the right *y* axis. **e**, Corresponding average increase in thermal sensor response from varying the temporal frequency of activation of LEDs illuminated at a duty cycle of 50%. **f**, Schematic of surgical implant of Opto-Array showing suturing of Opto-Array onto dura flap, sutured closing of dura mater and titanium strap cover on craniotomy. Credit: photographs in **a**, © 2020 Blackrock Microsystems, LLC

months, thus increasing the scale (number of trials, but also number of unique conditions) and throughput of causal experiments. Second, the two-dimensional (2D) matrix array configuration of LEDs enables the flexible perturbation of a large cortical region at fine resolution. Illuminating individual LEDs leads to focused perturbation of specific millimeter-scale regions, whereas simultaneously illuminating (arbitrary patterns of) multiple LEDs allows perturbation of larger cortical areas (currently up to 5 × 5 mm² for each array). Third, the Opto-Array provides a safe alternative to acute methods as well as direct illumination methods, minimizing the tissue damage that results from inserting large optical fibers into the cortical tissue, as well as the risk of infection associated with open cranial windows and chambers. Additionally, the Opto-Array includes an on-board thermal sensor to monitor heating (and potential damage) of the cortical tissue from light delivery. The key shortcomings of the optical array in its current format include its limitation to surface areas of the cortex (although implantation in large sulci and areas without direct visual access is possible) and its lack of neural recording probes. Furthermore, illumination from the surface of the brain is inherently biased towards superficial cortical layers[19], although this bias may be partly mitigated by the use of ultra-sensitive opsins[22,23]. Given the current challenges in behavioral optogenetics in large brains, we designed the first generation of Opto-Array specifically for behavioral experiments.

Each LED array consists of a 5 × 5 printed circuit board (PCB) grid with 24 LEDs (green 530-nm LEDs were used here) and one thermal sensor for monitoring tissue heating (Fig. 1a). Each LED is 0.5 × 0.5 mm², with 1-mm spacing between LEDs. The PCB and LEDs are encapsulated within a thin (<0.5 mm; total array thickness of 1.5 mm) translucent silicone cover. The LED array is designed to be chronically implanted directly on the cortical surface by suturing the silicone encapsulation onto the dura mater (Fig. 1). The LED array is powered through a thin gold wire bundle terminating on a Cereport pedestal connector that is implanted on the skull surface. Together, this implant allows for the delivery of light to a large region of the cortical surface with high spatial and temporal precision and stability over months of data collection, with minimal tissue proliferation underneath the array (Extended Data Fig. 1a).

We first characterized the photometric properties of the Opto-Array for direct comparison with an alternative light delivery method (Fig. 1b). Individual LEDs operating at 30% intensity match the power output of optical fibers that have yielded measurable behavioral effects in monkeys (10–15 mW). We then measured the spatial density of light power on the horizontal plane at a transverse distance of <1 mm from the surface of the LED (Fig. 1c). Given that light delivered from LEDs is not collimated, the spatial spread of light power over the horizontal plane is larger than the size of individual LEDs (full-width at half-maximum = 2.6 mm).
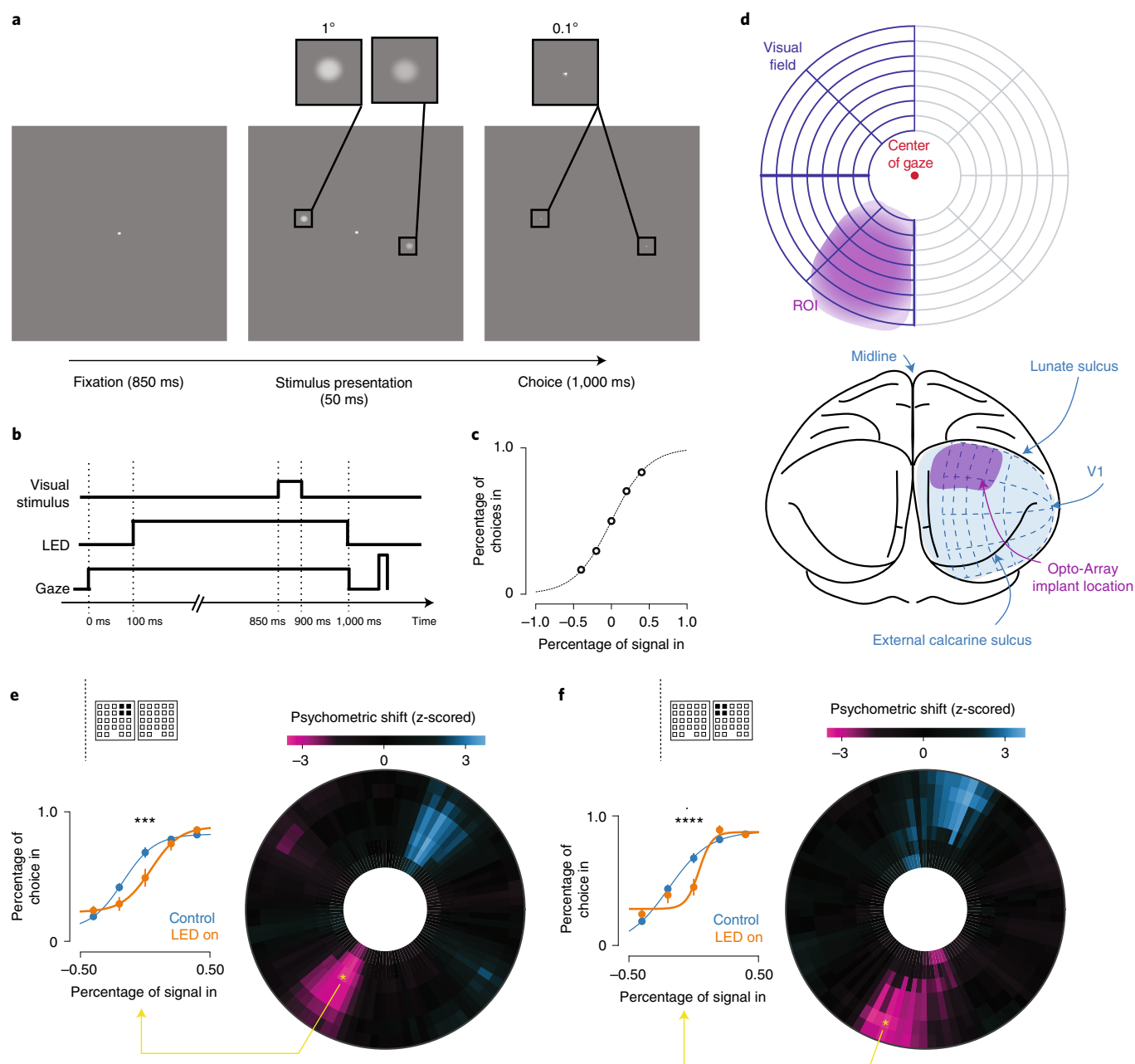
**Fig. 2 | Opto-Array design. a**, Behavioral paradigm for luminance discrimination task. **b**, The time course of the behavioral paradigm described in **a**. **c**, Control behavior, showing the psychometric relationship between the animal's choice (the proportion of choices into a given region of the visual field) and the visual stimulus signal (the difference in opacity between the stimulus in the given region of the visual field and the corresponding stimulus in the radially opposite region), pooling over all regions of the visual field. **d**, Correspondence between spatial organization of V1 cortex (bottom) and the visuospatial organization of the visual field (top). Behavioral effects from perturbing the Opto-Array implant region are expected to be spatially constrained to a target ROI, shown in purple. **e**, For one example LED condition (see top left inset for location of activated LEDs), the z-scored psychometric shift map is shown (right), with raw behavioral data (mean ± s.e.m. over trials; $n > 20$ trials for 'LED on' condition, $n > 60$ trials for 'control' condition) and fitted psychometric curves from the target regions shown on the left. **f**, Same as panel **e**, for a second example LED condition. Across all panels, asterisks are defined as: *$P < 0.05$, **$P < 0.01$, ***$P < 0.001$, ****$P < 0.0001$.

This extent of light spread corresponds to a relative attenuation of light power of 66% at a distance of 1 mm (one LED position apart) and of 20% at a distance of 2 mm (two LED positions apart). Finally, the Opto-Array output power was largely unaffected by implantation for several months, demonstrating in vivo viability of this tool (Extended Data Fig. 1b).

Next, we characterized the thermal response of the Opto-Array using the on-board thermal sensor. This measurement is

a conservative upper bound for the corresponding temperature change on the cortical surface, as each 1 °C increase measured by the thermal sensor corresponds to an estimated increase of <0.15 °C on the surface of the brain (Extended Data Fig. 1c–f). We aim to limit illumination-driven tissue heating because cortical temperature increases above 2 °C have been reported to induce spiking in some cell types in rodents[24], and increases above 4 °C can induce tissue damage[6]. The average increase in thermal sensor response,

and corresponding estimated increase on the brain surface, increase linearly as a function of the illumination energy (combining electrical power and illumination duration), both at a fixed low frequency of activation (Fig. 1d) and when varying the temporal frequency of activation (Fig. 1e), but remain well below the threshold for tissue damage. Together, these data demonstrate that the Opto-Array can measure heating caused by LED illumination, and also that typical experimental usage results in heating that is below the risks of tissue damage.

**Behavioral perturbation in macaque primary visual cortex (V1).**
We then tested the efficacy of the Opto-Array in vivo in a primate behavioral experiment. As a proof of concept, we investigated the causal role of mesoscale subregions in the V1 cortex of a macaque monkey in the context of a two-alternative forced-choice luminance discrimination task (Experiment 1; Fig. 2a,b). We trained a monkey to report the location of a visual target stimulus based on its luminance, in the presence of a distractor stimulus. By varying the relative luminance of the two stimuli, we systematically varied the task difficulty. The monkey's performance varied systematically with the task difficulty as expected (Fig. 2c), with increased probability of choosing a region of the visual field with increased visual signal (the difference in luminance between the stimulus in the region and the stimulus outside the region). We presented stimuli at randomly selected locations in the visual field within a fixed range of eccentricity, resulting in a disc of tested visual space. We then implanted two LED arrays over a dorsal region of the right V1 cortex, which was previously infected with AAV8-CAG-ArchT. We verified modest viral expression and neuromodulation via a small number of acute optrode experiments (Extended Data Fig. 2). Given the functional organization of V1 cortex, behavioral effects from perturbing this cortical region are expected to be spatially constrained on the visual field (target region of interest (ROI), contralateral lower visual field; Fig. 2d). A corresponding behavioral effect of equal magnitude and opposite sign is expected in the radially opposite position in the visual field by design, given the spatial symmetry of the task.

We measured the monkey's performance in the luminance discrimination task, comparing illumination versus control trials. To maximize both the spatial spread and power of light, we activated groups of four neighboring LEDs simultaneously, and interleaved four such groups. Given the chronic nature of the Opto-Array, we collected behavioral data over nine consecutive sessions while activating LEDs on a small portion of trials (20%). Pooling over all LED conditions and over the entire ROI, we observed a reliable behavioral effect of LED illumination even at this coarse scale, in the form of a statistically significant psychometric shift for a spatially restricted subregion of the visual field encompassed within the ROI ($P = 4.75 \times 10^{-4}$, one-tailed z-test; Extended Data Fig. 3). We then analyzed the corresponding effects over different LED conditions and different subregions within the target ROI by acquiring psychometric shift maps for two different example activation conditions (each of four neighboring LEDs; Fig. 2e,f). Each map shows a reliable behavioral shift at subregions of the visual field encompassed within the ROI ($P = 1.84 \times 10^{-4}, 3.67 \times 10^{-5}$, one-tailed z-test), where each effect is spatially restricted to a distinct subregion of the visual field encompassed within the ROI. These results demonstrate that, even in spite of the weak viral expression and weak optogenetic suppression of neural activity that we observed here, illumination from the Opto-Array results in reliable spatially restricted behavioral effects, validating this tool for behavioral experiments with optogenetic perturbation. The specific spatial illumination parameters necessary to induce different behavioral effects for different illumination conditions (for example, number of active LEDs per illumination condition, and the minimum distance between LEDs across illumination conditions) are critically dependent on the behavioral task, cortical area and viral expression levels. Here, we demonstrated a proof of concept for four LEDs and 2-mm cortical distance.

To rule out that the observed effects are the result of local cortical heating and not the intended physiological effects of the opsin, we additionally demonstrate in two separate experiments that illumination of virus-expressing cortical tissue via the Opto-Array results in neural suppression (Experiment 2; Extended Data Fig. 4) and that the behavioral effects of cortical illumination cannot be attributed to nonspecific effects such as tissue heating (Experiment 3; Extended Data Fig. 5).

In Experiment 2, we recorded neural activity from directly underneath the Opto-Array with a separate acute electrode, as the first generation of the Opto-Array does not include electrode contacts for simultaneous electrophysiology. Given that this experiment is not possible in area V1, we performed a separate experiment with a separate monkey in area IT (inferior temporal cortex (IT cortex)), using a high-resolution micro-focal stereo X-ray system[25] to precisely guide our electrodes close to the array surface (Extended Data Fig. 4a,b). We reconstructed the three-dimensional (3D) location of all recorded IT sites relative to the Opto-Array (Extended Data Fig. 4c,d) and characterized neural suppression from Opto-Array illumination, for both neighboring and distant IT neural sites (Extended Data Fig. 4e). Over all recorded neighboring neural sites, the neural suppression by light delivery was modest (up to ~6% on average) but statistically significant ($P < 0.01$, one-sided exact test). The suppression was not limited to the duration of illumination, suggesting that effects may at least in part be due to network-level effects. Distant IT sites did not show reliable suppression.

In Experiment 3, we implanted two LED arrays in left and right IT cortices of another animal, after transfecting one of the sides with virus (Extended Data Fig. 5a,b). We then trained the animal to behaviorally detect and report optogenetic cortical stimulation (Extended Data Fig. 5c). The animal was able to detect and report the activation of the Opto-Array on the opsin-expressing hemisphere (stimulation trials), but not on the control hemisphere (catch trials) (Extended Data Fig. 5d). We quantified this effect using data from the last five sessions of the experiment: the average report stimulation was 83.4%, 10.4% and 8.4% for stimulation, nonstimulation and catch trials, respectively, with a significant difference between the stimulation and nonstimulation trials ($X^2 (1, N = 4,249) = -47.8, P < 1 \times 10^{-12}$), but no statistically significant difference between the catch and nonstimulation trials ($X^2 (1, N = 2,834) = 1.3, P = 1.9 \times 10^{-1}$).

## Discussion
Together, our results demonstrate the potential utility of Opto-Array for optogenetic perturbation experiments in large primate brains. This tool improves the utility of optogenetics in large brains by advancing the method of light delivery and could be further enhanced in the future to include recording probes as well. The main limitation of Opto-Array stems from surface illumination that is inherently biased towards superficial cortical layers, and that renders access to deep brain structures difficult. In sum, we demonstrate that Opto-Array can help enable safer, chronically reproducible behavioral optogenetics experiments in NHPs, and may also serve as a platform for development of implantable prosthetic devices for the human brain.

## Online content
Any methods, additional references, Nature Research reporting summaries, source data, extended data, supplementary information, acknowledgements, peer review information; details of author contributions and competing interests; and statements of data and code availability are available at https://doi.org/10.1038/s41592-021-01238-9.

## References

1. Yizhar, O., Fenno, L. E., Davidson, T. J., Mogri, M. & Deisseroth, K. Optogenetics in neural systems. *Neuron* **71**, 9–34 (2011).
2. Deisseroth, K. Optogenetics: 10 years of microbial opsins in neuroscience. *Nat. Neurosci.* **18**, 1213–1225 (2015).
3. Jarvis, S. & Schultz, S. R. Prospects for optogenetic augmentation of brain function. *Front. Syst. Neurosci.* **9**, 157 (2015).
4. El-Shamayleh, Y. & Horwitz, G. D. Primate optogenetics: progress and prognosis. *Proc. Natl Acad. Sci. USA* https://doi.org/10.1073/pnas.1902284116 (2019).
5. Berdyyeva, T. K. & Reynolds, J. H. The dawning of primate optogenetics. *Neuron* **62**, 159–160 (2009).
6. Galvan, A. et al. Nonhuman primate optogenetics: recent advances and future directions. *J. Neurosci.* **37**, 10894–10903 (2017).
7. Diester, I. et al. An optogenetic toolbox designed for primates. *Nat. Neurosci.* **14**, 387–397 (2011).
8. Matsumoto, M., Inoue, K.-I. & Takada, M. Causal role of neural signals transmitted from the frontal eye field to the superior colliculus in saccade generation. *Front. Neural Circuits* **12**, 69 (2018).
9. Jazayeri, M., Lindbloom-Brown, Z. & Horwitz, G. D. Saccadic eye movements evoked by optogenetic activation of primate V1. *Nat. Neurosci.* **15**, 1368–1370 (2012).
10. Gerits, A. et al. Optogenetically induced behavioral and functional network changes in primates. *Curr. Biol.* **22**, 1722–1726 (2012).
11. May, T. et al. Detection of optogenetic stimulation in somatosensory cortex by non-human primates—towards artificial tactile sensation. *PLoS ONE* **9**, e114529 (2014).
12. Ozden, I. et al. A coaxial optrode as multifunction write-read probe for optogenetic studies in non-human primates. *J. Neurosci. Methods* **219**, 142–154 (2013).
13. Acker, L., Pino, E. N., Boyden, E. S. & Desimone, R. FEF inactivation with improved optogenetic methods. *Proc. Natl Acad. Sci. USA* **113**, E7297–E7306 (2016).
14. Dai, J. et al. Modified toolbox for optogenetics in the nonhuman primate. *Neurophotonics* **2**, 031202 (2015).
15. Sileo, L. et al. Tapered fibers combined with a multi-electrode array for optogenetics in mouse medial prefrontal cortex. *Front. Neurosci.* **12**, 771 (2018).
16. Ruiz, O. et al. Optogenetics through windows on the brain in the nonhuman primate. *J. Neurophysiol.* **110**, 1455–1467 (2013).
17. Chernov, M. M., Friedman, R. M., Chen, G., Stoner, G. R. & Roe, A. W. Functionally specific optogenetic modulation in primate visual cortex. *Proc. Natl Acad. Sci. USA* **115**, 10505–10510 (2018).
18. Yazdan-Shahmorad, A. et al. A large-scale interface for optogenetic stimulation and recording in nonhuman primates. *Neuron* **89**, 927–939 (2016).
19. Chuong, A. S. et al. Noninvasive optical inhibition with a red-shifted microbial rhodopsin. *Nat. Neurosci.* **17**, 1123–1129 (2014).
20. Yazdan-Shahmorad, A. et al. Demonstration of a setup for chronic optogenetic stimulation and recording across cortical areas in non-human primates. In *Proceedings Volume 9305, Optical Techniques in Neurosurgery, Neurophotonics, and Optogenetics II* (ed. Hirschberg, H.) 93052K (International Society for Optics and Photonics, 2015).
21. Komatsu, M., Sugano, E., Tomita, H. & Fujii, N. A chronically implantable bidirectional neural interface for non-human primates. *Front. Neurosci.* **11**, 514 (2017).
22. Gong, X. et al. An ultra-sensitive step-function opsin for minimally invasive optogenetic stimulation in mice and macaques. *Neuron* **107**, 38–51.e8 (2020).
23. Marshel, J. H. et al. Cortical layer–specific critical dynamics triggering perception. *Science* **365**, 6453 (2019).
24. Owen, S. F., Liu, M. H. & Kreitzer, A. C. Thermal constraints on in vivo optogenetic manipulations. *Nat. Neurosci.* **22**, 1061–1065 (2019).
25. Cox, D. D., Papanastassiou, A. M., Oreper, D., Andken, B. B. & Dicarlo, J. J. High-resolution three-dimensional microelectrode brain mapping using stereo microfocal X-ray imaging. *J. Neurophysiol.* **100**, 2966–2976 (2008).

## Methods

All animal procedures were approved by the National Institute of Mental Health Animal Care and Use Committee, and were performed in compliance with National Institutes of Health guidelines and the standards of the Massachusetts Institute of Technology Committee on Animal Care and the American Physiological Society.

**Specifications of Opto-Array and Driver.** The Opto-Array consists of a pair of LED arrays connected to a skull-mounted pedestal, which is itself powered by an external LED Driver connected to a controller computer (Fig. 1a). The full specifications for the Opto-Array and LED Driver are listed in Supplementary Table 2 and Supplementary Table 3, respectively. Arrays and drivers were manufactured by Blackrock Microsystems. In the current study, we used Opto-Arrays with Cereport connectors with 13-cm wire bundles, and green LEDs (530 nm).

**Photometric measurements.** Photometric measurements were made with a power-meter (Thorlabs Digital Handheld Optical Power and Energy Meter Console) coupled to a slim photodiode power sensor, placed in tight proximity (<0.5 mm) to the surface of the LED arrays, mimicking the distance between the sutured LED array and the cortical surface. We averaged the power output over a sensor of 9 mm in diameter and over a 500-ms duration window. We additionally repeated this experiment on an Opto-Array that was implanted in an animal for 155 d. The light output of the explanted array approximately matched that of a new one (Extended Data Fig. 1b), demonstrating the survivability of this tool in vivo.

To measure the spatial density of LED power, we measured the power output of individual LEDs with the same power-meter, but with a pinhole occluder placed in between, with varying pinhole size. We first manually aligned the center of the LED array to the pinhole using a manual stage (Thorlabs). We then measured the light power from each individual LED on the array separately, repeated ten times. We then selected the individual LED that was best aligned with the pinhole (that is, the LED with maximally detected power). Importantly, we cannot measure the extent of light propagation in tissue along the third dimension (depth) using such photometric measurements, given the importance of light absorption and light scattering in brain tissue. Instead, we refer to published Monte Carlo simulations that report the profile of light fluence as a function of the distance from the light source[19]. These simulations predict that approximately 30% of the peak light power penetrates a depth of 1 mm for green light.

**Temperature measurements.** We measured the thermal response of an Opto-Array implanted directly on the cortical surface of an adult rhesus monkey in two separate experiments. Temperature was sampled from the embedded thermistor every 30 ms. As described below, this measurement provides a conservative upper bound for the corresponding temperature change on the cortical surface, given the silicone insulation that separates the thermistor from the brain. It is also worth mentioning that temperature readings vary depending on the distance of each LED from the thermistor on the PCB. To factor out the apparent thermal effect of LED distance from the thermistor we used only the LEDs that are adjacent to the thermistor. To ensure the animal's safety, in both experiments, trials in which the PCB temperature increased more than 3 °C were aborted.

In experiment 1, we measured the LED thermal response after a single activation (that is, an activation followed by a long pause, in contrast to a sequence of activations). Each trial lasted for 11 s and contained one activation that started 1 s after the onset of the trial. Each activation condition was randomly selected from a set of combinatory conditions including the following parameters: the number of active LEDs (1, 3 or 5), duration of activation (100, 200 or 500 ms) and electrical power of activation (0, 40, 82 or 132 mW). Each trial type was repeated ten times, except for the trials in which the temperature crossed the 3 °C safety limit (Extended Data Fig. 1c).

In experiment 2, we measured the thermal response during sequences of LED activations. Each trial started with recording 1 s of baseline temperature before sequences of LED activations that each lasted 10 min. Each activation sequence was randomly selected from a set of 40 combinatory conditions including the following parameters: the number of active LEDs (1 or 5), duration of activation (200 ms or 500 ms), power of activation (82 or 191 mW) and duty cycle of activation (one pulse every 1, 2, 4, 8 or 16 s).

Given the measured temperature changes on the Opto-Array, we estimated the corresponding temperature changes on the surface of the brain by solving the heat equation using a finite-element model analysis (Extended Data Fig. 1d). Finite-element modeling was performed using MATLAB (MathWorks). For simplicity, we considered a 2D cross-section of the array on the brain surface and built a 2D surface consisting of a PCB contained within a silicone encapsulation, adjacent to brain tissue (Extended Data Fig. 1d). We used the following thermal properties for the silicone encapsulation: thermal conductivity = 0.2 W m$^{-1}$ K$^{-1}$, mass density = 1,200 kg m$^{-3}$ and specific heat = 1,300 J kg$^{-1}$ K$^{-1}$. Similarly, we used the following thermal properties for the brain tissue: thermal conductivity = 0.51 W m$^{-1}$ K$^{-1}$, mass density = 1,100 kg m$^{-3}$ and specific heat = 3,630 J kg$^{-1}$ K$^{-1}$. We set the boundary conditions of the PCB-to-silicone edge to match the time course of measured temperature changes and simulated the time

course of temperature over the array and brain surface (Extended Data Fig. 1e). Our simulations suggest that each 1 °C increase measured by the thermal sensor corresponds to an estimated increase of <0.15 °C on the surface of the brain.

**Subjects and surgery (Experiment 1).** Behavioral data were collected from one adult male rhesus macaque monkey (*Macaca mulatta*, subject Y). Monkey Y was implanted with a titanium head post to the skull under aseptic conditions and was trained on a two-alternative forced-choice luminance discrimination task (Fig. 2a,b) under head-fixation using standard operant conditioning (fluid reward). Following this, we performed a sterile surgery for virus injection. Following a craniotomy on the right hemisphere of the V1 cortex, we injected AAV8-CAG-ArchT through the dura over a region of 15 × 7 mm$^2$. We injected in 12 distinct injection sites on the cortical surface, spaced approximately 2.5–3 mm apart. At each site, we injected 1 µl at a rate of 200 nl min$^{-1}$ at three depths spaced approximately 0.5 mm apart, starting from the deepest level and pulling up gradually, for a total of 3 µl per site. To cover this relatively large region evenly, we used a thin plastic grid overlay (termed 'Schmidt grid') with evenly spaced holes that we affixed to the bone to guide the injection needles through. Following injection, the craniotomy was covered by a titanium mesh, and the fascia and skin were sutured closed.

Several months after the virus injection surgery, we performed another surgery to verify viral expression and implant a recording chamber. We performed a durotomy over the target area and used fluorescence imaging to confirm virus expression. Specifically, we turned off the lights of the operating room and used a flashlight with appropriate wavelength and proper goggles (for example, 440–460-nm excitation light, 500-nm longpass filter for GFP) to directly inspect and photograph the fluorescence of the viral expression zone. Besides confirming the viral expression, one advantage of this method is to visualize the expression zone and implant the array precisely over it. Using this method, we observed poor expression. We sutured the dura mater closed and implanted a steel recording chamber (Crist) for acute optrode experiments (see below). We did this to test for viral expression using a traditional method, but this stage is not typically needed. We recommend covering the viral injection zone with artificial dura before closing the dura on it. The layer of artificial dura (between pia and dura) prevents tissue adhesion in the period between virus injection and array implantation.

In a subsequent surgery, we removed the chamber and implanted two 5 × 5 LED arrays over the transfected tissue. Localization of the array implant locations was done using landmarks of the location of the craniotomy, such that array locations were nearly overlapping the location of the recording chamber, and thus in proximity to the previously performed optic fiber experiments. To provide access for array implantation, a large U-shaped incision (5 × 10 mm$^2$, base of the U being the long side) was made in the dura mater. The array was kept in position by suturing the holes in the corners of the arrays to the edges of the rectangular opening in the dura (using nonabsorbable suture). This keeps the arrays tightly aligned with the pia surface directly under them. The dura flap was loosely sutured over the arrays (to avoid putting pressure on the cortex) and the area was covered with DuraGen. Schematics of this surgical procedure are shown in Fig. 1f.

We explanted the Opto-Array after 155 d implanted in monkey Y and observed little to no necrotic tissue proliferation on the cortex under the arrays (Extended Data Fig. 1a). Furthermore, the light output of the explanted array approximately matched that of a new one (Extended Data Fig. 1b). Together, these observations demonstrate the survivability of this tool in vivo.

We infer that viral expression in the V1 cortex of monkey Y was weak based on (1) little to no fluorescence observed in surgery (using the method described above), and (2) weak but statistically significant neural modulation from direct physiological recording (with ~5–20% spikes suppressed), measured using an acutely inserted optic fiber coupled to a green light laser (Extended Data Fig. 2). Given that the latter confirmed the existence of modest viral expression, we did not perform any histological analyses.

**Behavioral paradigm (Experiment 1).** The luminance discrimination behavioral task was designed to probe the role of millimeter-scale regions of V1 cortex, which encode local features of the visual field. Stimuli were presented on a 24″ LCD monitor (1,920 × 1,080 at 60 Hz; Acer GD235HZ) and eye position was monitored by tracking the position of the pupil using a camera-based system (SR Research Eyelink 1000). At the start of each training session, the subject performed an eye-tracking calibration task by saccading to a range of spatial targets and maintaining fixation for 800 ms. Calibration was repeated if drift was noticed over the course of the session.

Each trial of the behavioral task consisted of a central visual fixation period, during which the animal had to hold gaze fixation on a central fixation spot for 900 ms (Fig. 2a). On a random proportion of trials, a subset of LEDs were pre-emptively activated during this epoch. This was followed by the simultaneous and brief (50 ms) presentation of two sample stimuli in the periphery, at radially opposite locations in the visual field. Stimulus images spanned 1° of visual angle in size, and consisted of clipped Gaussians with a standard deviation of 0.6° of visual angle. The stimulus luminance was controlled via the opacity of the presented image (alpha between 0% and 100%). LED activation was timed to completely overlap the stimulus-related activity in V1 cortex. Following the extinction of these

stimuli, two target dots were presented at the stimulus locations. The task required the subject to make a saccade to a target location defined by the brighter of the two sample stimuli. The location of the target was randomly sampled on each trial by sampling a random radius $r$ (between 3° and 10°) and angle theta (between 0 and $2\pi$). By varying the relative luminance of the two sample stimuli (here defined as the difference in opacity alpha between the target and distractor stimuli), we systematically varied the task difficulty. We tested four different LED conditions, each consisting of the simultaneous activation of four neighboring LEDs; these four conditions, along with the no-light control condition, were interleaved randomly trial-by-trial. Correct reports were rewarded with a juice reward. To control the temperature on the Opto-Array and on the brain, we imposed a temperature-dependent criterion, whereby increases in temperature greater than 3 °C, as measured by the on-board thermistor, automatically led to a pause in the behavioral task. Real-time experiments for monkey psychophysics were controlled by open-source software (MWorks Project http://mworks-project.org/). Behavioral analysis was performed using Python 3.6, relying on numpy, scipy and pandas libraries.

**Optical fiber experiments (Experiment 1).** To provide a baseline for comparison across methodologies, we first performed a small number of acute optical fiber experiments. We first confirmed weak viral expression by recording modest neural modulation by delivery of green light via an acutely inserted optical fiber (Extended Data Fig. 2). Next, we measured the behavioral effects of optogenetic suppression with light delivered via an acutely inserted fiber.

**Opto-Array experiments (Experiment 1).** Behavioral data with LED activation were collected over nine behavioral sessions, with $1,792 \pm 346$ (mean ± s.d.) trials per session. For the first set of experiments, we activated groups of four neighboring LEDs simultaneously to increase both the spatial spread and power of light. We interleaved four such groups, each consisting of four corners of arrays. Given the chronic nature of this tool, we pooled behavioral data over all sessions while activating LEDs on a small (20%) portion of trials, with the same illumination (900 ms) duration that yielded neural suppression and behavioral effects in optrode experiments.

**Behavioral analysis (Experiment 1).** To assess the behavioral effects from stimulation, we fit psychometric functions to the animal's behavioral choices, separately for each LED condition (including the control condition of no LED illumination), and for each tested position in the visual field. For each tested location (parameterized in polar coordinates with $r$, $\theta$), we pooled all trials where either of the target or distractor stimuli were presented in a pooling region spanning 4° along the radial dimension and $\pi/8$ along the angular dimension. For this subset of trials, we fitted a psychometric curve for each LED condition using logistic regression:

$$f(x) = \lambda_0 + \frac{\lambda_1}{1 + e^{-(\alpha + \beta x)}}$$

where $\lambda_0$, $\lambda_1$, $\alpha$ and $\beta$ are the fitted parameters and $f(x)$ and $x$ correspond to the dependent and experimentally controlled variables. $x$ corresponds to the visual signal, the difference in opacity between the stimulus in the pooling region and the stimulus outside the pooling region, on each trial. $f(x)$ models the choice, 1 for choice in the pooling region, 0 for choice outside the pooling region, on each trial. $\lambda_0$ and $\lambda_1$ model lapses, that is, the floor and ceiling values of the psychometric function, attributed to visual deficits not resulting from LED illumination. $\alpha$ and $\beta$ model the criterion and sensitivity of the psychometric function. We fit psychometric functions with constrained nonlinear least squares using standard Python libraries (scipy.curve_fit) and extracted both the fitted parameter estimates (for example, $\hat{\alpha}_{LED}$) and the variance of parameter estimates (for example, $\sigma^2_{\alpha_{LED}}$).

To assess the effect of LED activation, we measured the change in psychometric criterion (that is, corresponding to shifts in the psychometric curves) via the difference in estimated criterion between the function fits of the LED condition and the control condition: $\delta = \hat{\alpha}_{LED} - \hat{\alpha}_{control}$. We normalized this difference by the pooled variance $\sigma = \sqrt{\sigma^2_{\hat{\alpha}_{LED}} + \sigma^2_{\hat{\alpha}_{control}}}$ to obtain a z-scored metric: $z = \frac{\delta}{\sigma}$. Repeating this procedure for each tested location in the visual field, we obtained a 2D map of z-scored psychometric shift estimates. Z-scores were converted to one-tailed $P$ values using the survival function of the normal distribution $N(0,1)$, corresponding to a one-tailed z-test. We additionally report the corresponding change in all four psychometric parameters, $\lambda_0$, $\lambda_1$, $\alpha$ and $\beta$, in Extended Data Fig. 3c.

We used an ROI based on the functional organization of primate V1 cortex: the dorsal region of V1 cortex on the right hemisphere is known to represent the contralateral (left) lower visual field. Given that viral expression in monkey Y was verified to be poor and likely inhomogeneous over the cortical tissue, we did not attempt to localize behavioral effects from LED illumination with finer precision.

**Subjects and surgery (Experiment 2).** Data were collected from one adult male rhesus macaque monkey (*M. mulatta*, subject M). A surgery using sterile technique was performed under general anesthesia to implant a titanium head post to

the skull using titanium screws, and a cylindrical recording chamber (19-mm inner diameter; Crist) over a craniotomy targeting the temporal lobe in the left hemisphere from the top of the skull (+13 mm posterior-anterior, +16.3 mm medial-lateral, 15 degree medial-lateral angle).

Following this, we performed a sterile surgery for virus injection in the left IT cortex. Following a craniotomy on the left hemisphere, we injected AAV8-CAG-ArchT through the dura over a region of $15 \times 7$ mm². We injected in nine distinct injection sites on the cortical surface, spaced approximately 2.5 mm apart. At each site, we injected 2 µl at a rate of 600 nl min⁻¹ at two depths spaced approximately 1 mm apart, starting from the deepest level and pulling up gradually, for a total of 4 µl per site. To cover this relatively large region evenly, we used the aforementioned Schmidt grid to guide injection locations. Following injections, the craniotomy was covered by a titanium mesh, and the fascia and skin were sutured closed.

Several months after the virus injection surgery, we performed another surgery to verify viral expression and implant the Opto-Array over the IT cortex. We performed a durotomy over the target area, and used fluorescence imaging to confirm virus expression, as with monkey Y (see above). We observed strong fluorescence over a large region of the lateral IT cortex, and we implanted one Opto-Array over this localized target region. The second Opto-Array was cut off from the Cereport pedestal, and the dura mater was sutured closed.

All procedures were performed in compliance with National Institutes of Health guidelines and the standards of the Massachusetts Institute of Technology Committee on Animal Care and the American Physiological Society.

**Physiology (Experiment 2).** To accurately measure the relative positions of IT cortex recording locations relative to the implanted Opto-Array (Extended Data Fig. 3a), all electrophysiological recordings were made under micro-focal stereo X-ray guidance[25]. Briefly, at each site, two X-rays were taken simultaneously at near orthogonal angles, and the 3D location of the electrode tip was reconstructed relative to the Opto-Array using stereo-photogrammetric techniques (Extended Data Fig. 3b). Typically, this reconstruction is done relative to an external fiducial frame attached to the animal's head, but here we used the internally placed Opto-Array for an even more accurate reference frame. This procedure enables high-resolution reconstruction (~200-µm error) of electrode locations across experimental sessions[25,26].

We recorded multi-unit activity from randomly sampled sites on the lateral surface of IT cortex while monkey M passively fixated images in a rapid serial visual presentation protocol (10 images per trial, 100 ms on, 100 ms off). Naturalistic synthetic images of basic-level objects were shown at a size of 8° of visual angle. Recordings were made using glass-coated tungsten micro-electrodes (impedance, 0.3, 0.5 MΩ; outer diameter, 310 µm; Alpha Omega). A motorized micro-drive (Alpha Omega) was used to lower electrodes through a 26-gauge stainless-steel guide tube inserted into the brain (5 mm) and held by a plastic grid inside the recording chamber (Crist). We randomly interleaved trials with and without light delivery from the chronically implanted Opto-Array, with LED illumination aligned to [−50 ms, +190 ms] relative to image onset. To ensure accurate stimulus presentation, eye position was tracked, and trials were aborted if gaze was not held within ±1.5° of visual angle. To ensure accurate stimulus locking, spikes were aligned to a photodiode trigger attached to the display screen. Multi-unit responses were amplified (1× head-stage), filtered (250-Hz cutoff), digitized (sampling rate of 40 kHz) and sorted (Plexon MAP system, Plexon).

To assess neural suppression over the recorded population, we split all neural sites into two groups based on the 3D distance between the site location and the location of the illuminated LED ('neighboring' and 'distant' sites, defined as less than and greater than the median distance over all sites, respectively).

**Subjects and surgery (Experiment 3).** Data were collected from one adult male rhesus macaque monkey (*M. mulatta*, subject S). We used an excitatory opsin (C1V1) to stimulate the central temporal (TE) area of the IT cortex. The surgical procedure was similar to the V1 cortex experiment except we used a multi-channel injection array for uniform viral injection on the cortical surface[27]. After durotomy on the left hemisphere, we injected AAV5-CaMKIIa-C1V1(t/t)-EYFP (nominal titer: $8 \times 10^{12}$ particles per ml) in 14 injection tracks approximately covering a region of $8 \times 8$ mm²; 10 µl was injected at each site, at a rate of 0.5 µl min⁻¹. After 3 months, we performed the second durotomy and confirmed the virus expression by documenting the fluorescence produced by YFP on the cortical surface. In the same surgery, we implanted a pair of Opto-Arrays: one over the injection zone, the other in a similar position (central IT cortex) in the opposite hemisphere where no virus injection was performed (Extended Data Fig. 5c). After 4 weeks of recovery, we started the behavioral experiment. All procedures were reviewed and approved by the National Institute of Mental Health Animal Care and Use Committee.

**Behavioral paradigm (Experiment 3).** In this experiment, the animal was trained to detect optogenetic stimulation of its IT cortex (Extended Data Fig. 5a,b). Each trial started by presenting a central fixation point (black-on-white bullseye, 0.4° outer diameter, 0.2° inner diameter) on a gray background. Following 500 ms of fixation, a visual stimulus (for example, a picture of a butterfly) was presented on the screen for 1 s. Over the course of the training, the content, distribution

and size of these visual stimuli were varied, but in all cases the same set of visual stimuli was shown in all stimulation conditions and the visual stimulus was not predictive of the stimulation condition. The animal was trained not to break the fixation and only report the Opto-Array activation, independent from the choice of visual stimuli. In 50% of the trials (randomly selected) no optical stimulation was delivered to the cortex ('no-stimulation trials'). In the other 50% of the trials, five LEDs of the Opto-Array were activated, midway through the visual stimulus presentation, for 200 ms at 12-mW light power each. In 80% of the LED-activated trials, the optical stimulation was delivered to the transfected cortex ('stimulation trials', 40% of total); for the rest of the trials ('catch trials', 10% of total), the intact cortex (with no virus injection) was illuminated with the same illumination parameters.

The fixation point then disappeared and two choice targets (white, 0.4° diameter) appeared simultaneously on the vertical midline 5° above and below the fixation position. The animal's task was to report if the trial contained IT cortex stimulation by fixating on one of the targets for 100 ms (the bottom target was assigned to stimulation trials and vice versa). We treated stimulation and catch trials equally in our reward schema so that the animal would receive reward for reporting both stimulation and catch trials as 'stimulated'. The animal received liquid reward for correctly selecting the choice target that corresponded to the trial type. Performance on catch trials would reveal if the animal was using heating of the cortex, or scatter of light inside the skull (potentially hitting the retinae from the back), to detect activation of the Opto-Array. The three trial types were presented in random order.

After observing extreme choice bias, on the thirteenth day of training we introduced a 'bias correction loop' procedure[28]. If the monkey made three consecutive incorrect choices in one direction, the monkey entered a 'correction loop' where all trials presented were of that same type. This lasted until the monkey selected the correct choice after which trials returned to being randomly interleaved. In the 5 d after introducing the correction loop the monkey spent as much as 75% of trials in correction loops. This quickly dropped to less than 10% after 5 more days and by the end of training correction loop trials made up less than 1% of trials. 'Stimulation' correction loops only contained stimulations over virus-expressing tissue. Data from correction loops are excluded from analysis in Extended Data Fig. 5d.

**Reporting Summary.** Further information on research design is available in the Nature Research Reporting Summary linked to this article.

## Data availability
The photometric, thermal and behavioral measurements used in this study are available at https://github.com/RishiRajalingham/NatureMethods2021.

## Code availability
The code used to generate behavioral analyses is available at https://github.com/RishiRajalingham/NatureMethods2021.

## References
26. Issa, E. B., Papanastassiou, A. M. & DiCarlo, J. J. Large-scale, high-resolution neurophysiological maps underlying fMRI of macaque temporal lobe. *J. Neurosci.* **33**, 15207–15219 (2013).
27. Fredericks, J. M. et al. Methods for mechanical delivery of viral vectors into rhesus monkey brain. *J. Neurosci. Methods* **339**, 108730 (2020).
28. Salzman, C. D., Murasugi, C. M., Britten, K. H. & Newsome, W. T. Microstimulation in visual area MT: effects on direction discrimination performance. *J. Neurosci.* **12**, 2331–2355 (1992).

## Author contributions
A.A. developed the concept and general characteristics of the Opto-Array. M.S. designed and fabricated the Opto-Array, with guidance from A.A. and J.J.D. R.R. performed the Opto-Array photometric experiments. S.B. and R.A. performed the Opto-Array thermal experiments, with guidance from A.A. R.R. and A.A. performed the optical fiber experiments, with guidance from J.J.D. R.R. performed the Opto-Array behavioral experiments in V1 cortex in monkey Y, with guidance from A.A. and J.J.D. R.R. performed the Opto-Array neural experiments in IT cortex in monkey M, with guidance from A.A. and J.J.D. S.B. and R.A. performed the Opto-Array behavioral experiments in IT cortex in monkey S, with guidance from A.A. R.R. and A.A. wrote the manuscript. All authors reviewed the manuscript.

## Competing interests
M.S. is a principal engineer at Blackrock Microsystems (Utah). Blackrock will sell the Opto-Array and is bound to financially benefit from this work.

## Additional information
**Extended data** is available for this paper at https://doi.org/10.1038/s41592-021-01238-9.

**Supplementary information** The online version contains supplementary material available at https://doi.org/10.1038/s41592-021-01238-9.

**Correspondence and requests for materials** should be addressed to A.A.

**Peer review information** *Nature Methods* thanks Adriana Galvan, Atsushi Nambu and the other, anonymous, reviewer(s) for their contribution to the peer review of this work. Nina Vogt was the primary editor on this article and managed its editorial process and peer review in collaboration with the rest of the editorial team.

**Reprints and permissions information** is available at www.nature.com/reprints.
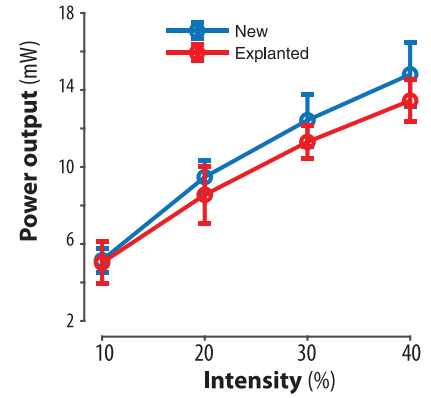
## A    Opto-Array explant
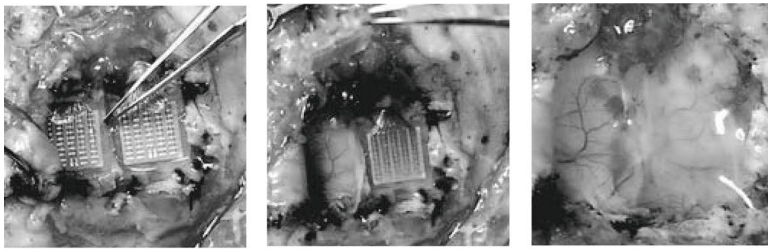


Dura mater opened, arrays exposed.

Medial array removed, cortex underneath exposed.
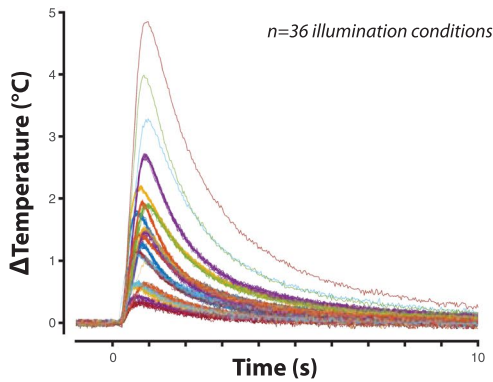
Both arrays removed, cortex underneath exposed.
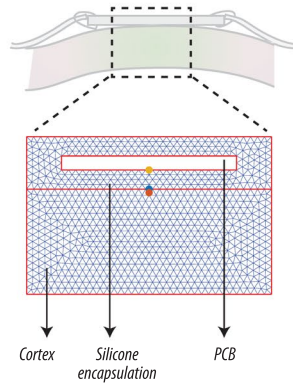
## B    Opto-Array survivability



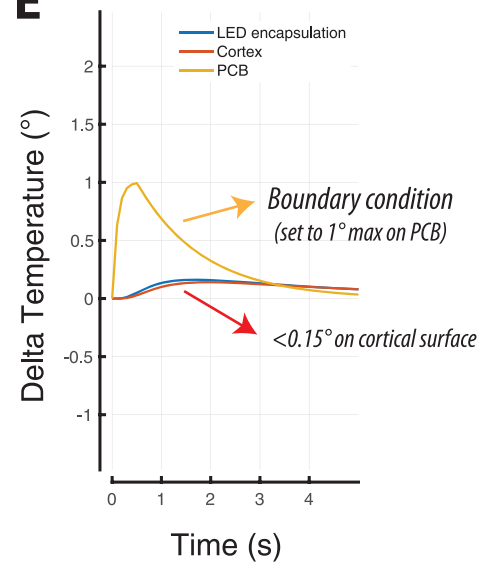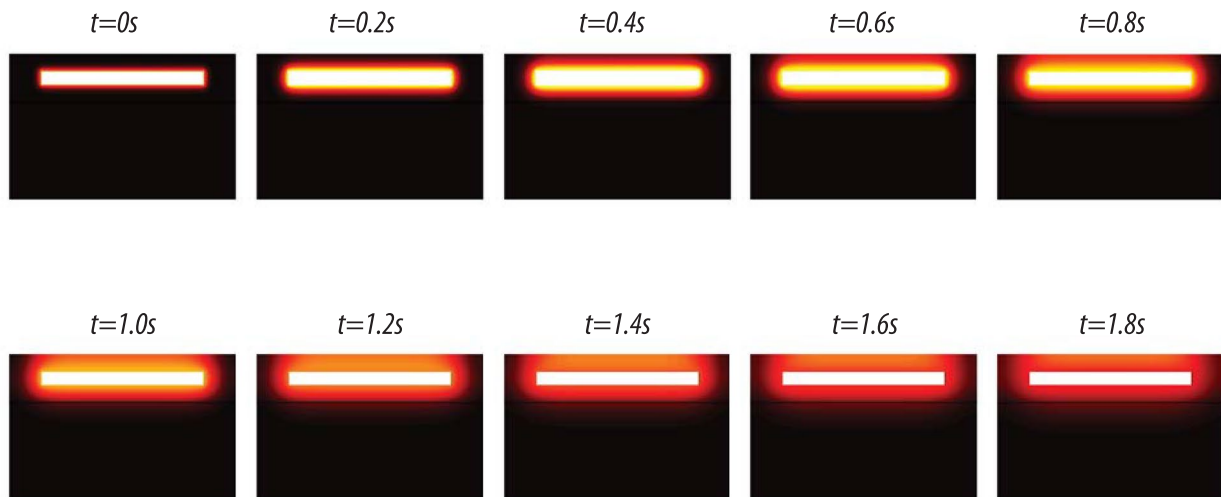## C    Empirical Opto-Array temperature response



*n=36 illumination conditions*

## D    Finite element model



## E



## F



t=0s    t=0.2s    t=0.4s    t=0.6s    t=0.8s

t=1.0s    t=1.2s    t=1.4s    t=1.6s    t=1.8s

**Extended Data Fig. 1 | See next page for caption.**

**Extended Data Fig. 1 | Thermal response.** (**a**) Photographs of the brain surface after explantation of Opto-Array after 155 days implanted in monkey Y. The photographs show the skull with craniotomy and durotomy over the right dorsal V1. The brain surface under each array is exposed and photographed. (**b**) Comparison of the light power output of a new Opto-Array to one that was implanted in an animal for 155 days (mean +- SD over repetitions, n = 80 repetitions). (**c**) Average thermal response from implanted Opto-Array to 36 different LED conditions, varying in power, duration, and number of illuminated LEDs. (**d**) Finite element model for simulating the temperature changes on the surface of the brain by solving the heat equation. For simplicity, we considered a 2D cross-section of the array on the brain surface and built a 2D surface consisting of a PCB contained within a silicone encapsulation, adjacent to brain tissue (top). (**e**) Temperature increases on the silicone encapsulation (blue) and the brain surface (red) after setting the boundary conditions of the PCB-to-silicone edge (yellow). (**f**) The simulated time course of temperature changes over the array and brain surface at 200 ms intervals.
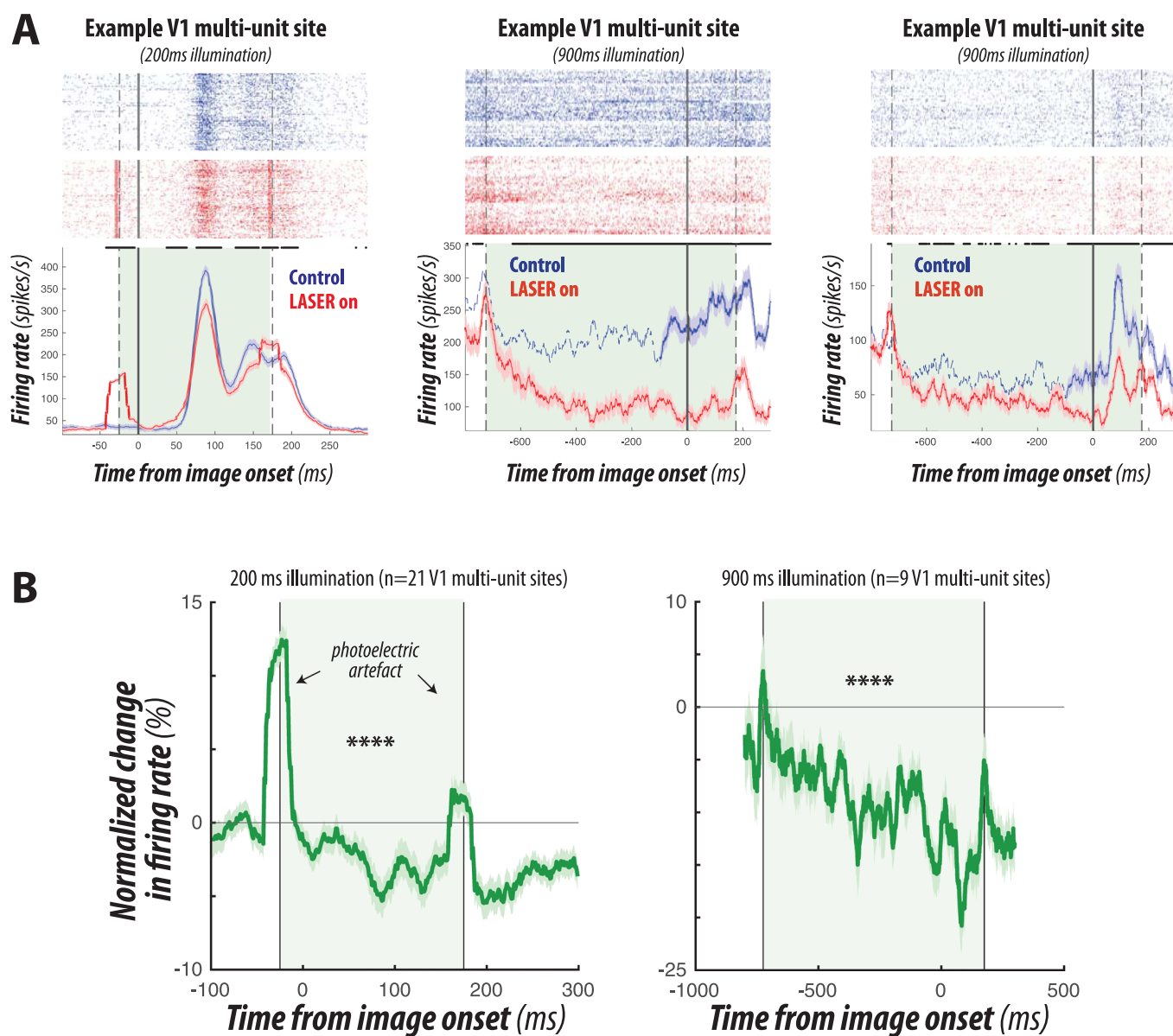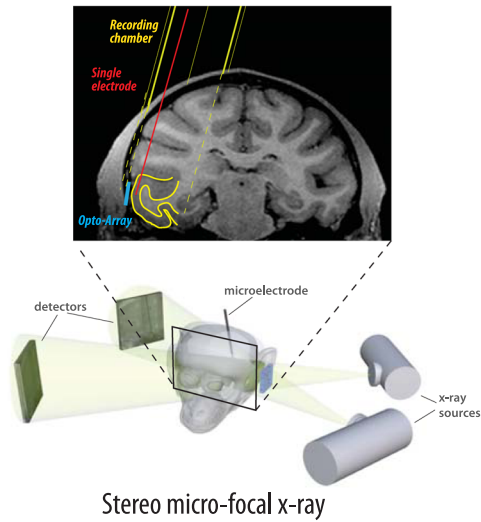
**Extended Data Fig. 2 | Neural suppression using optrodes in V1 cortex.** We recorded V1 responses to a brief full-field grating stimulus, shown under a rapid serial visual presentation (RSVP) protocol, interleaving trials with and without light delivery from the acutely inserted optic fiber coupled to a green light laser. (**a**) Example rasters and peri-stimulus time histograms (PSTHs) from fiber optic experiments for 200 ms light duration (left) and 900 ms light duration (middle, right). Note the presence of a photoelectric artefact during light onset and offset in the left panel. Shaded lines correspond to mean + - SE, over n > 30 repetitions. (**b**) The percentage change in neural response between laser ON and control conditions, averaged over all recorded neural sites. Shaded lines correspond to mean + - SE, over n = 21 multi-unit sites (left) and n = 9 multi-unit sites (right). The green overlays correspond to the time of LED illumination. Over all recorded neural sites, the neural suppression by light delivery was statistically significant (p < 0.0001, one-sided exact test). Across all panels, asterisks are defined as: *p < 0.05, **p < 0.01, ***p < 0.001, ****p < 0.0001.
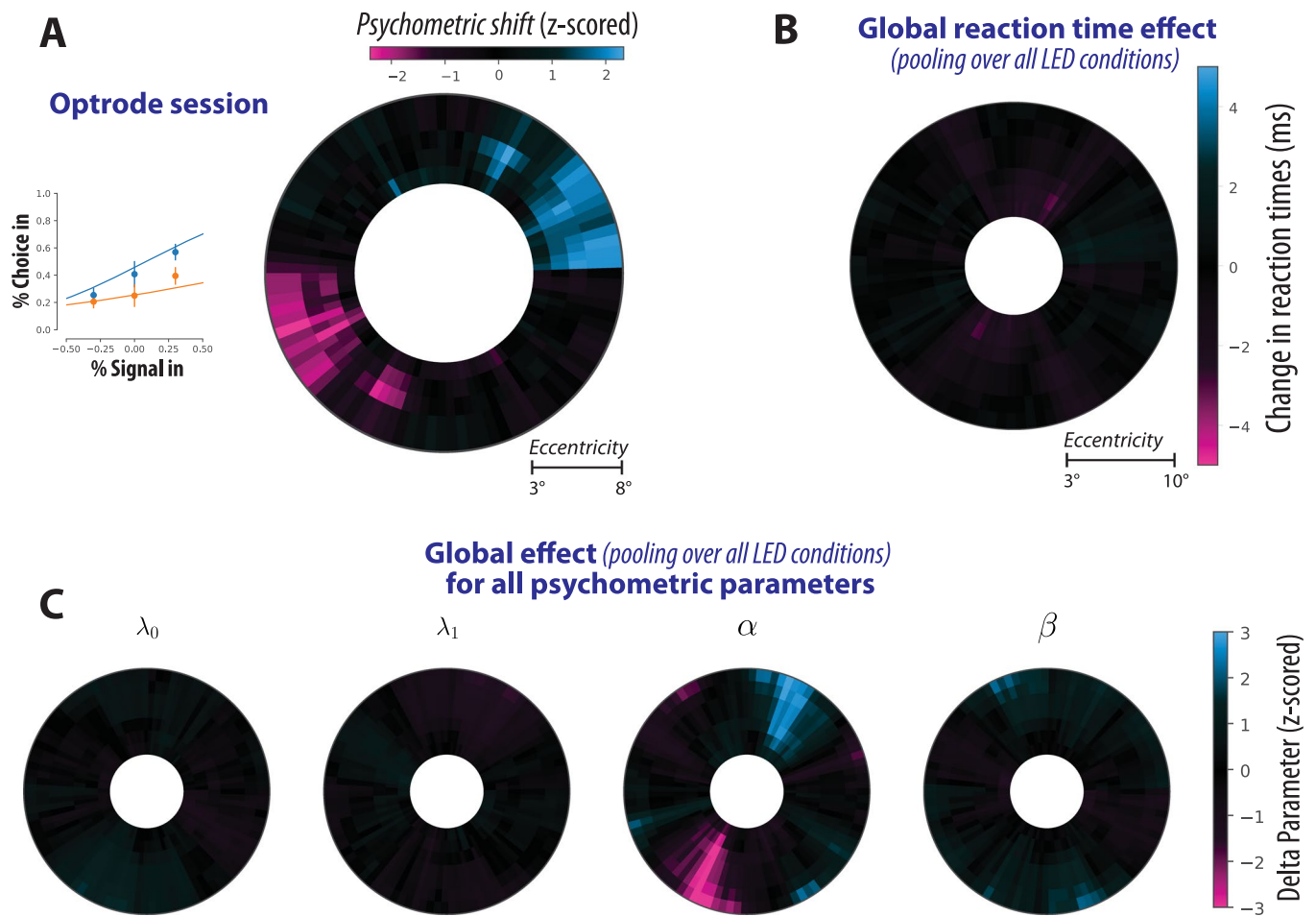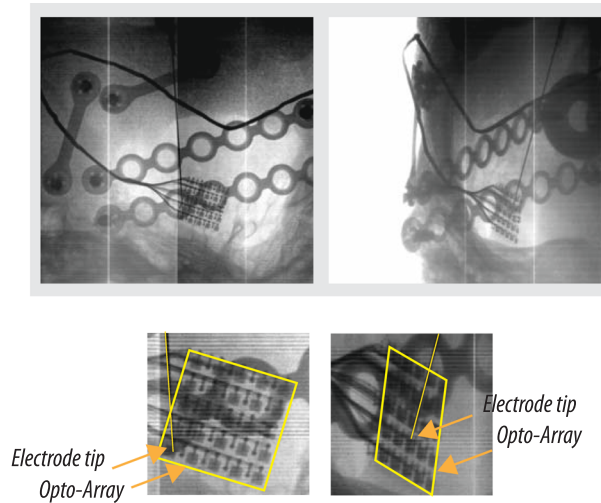
**Extended Data Fig. 3 | Behavioral effects of optogenetic suppression in V1 cortex.** (**a**) Behavioral effects of optogenetic suppression of V1 cortex with light delivered via an acutely inserted fiber, for the luminance discrimination task in monkey Y. Formatting as in Fig. 2e,f. We observe substantial psychometric shifts in the region of interest within the visual field (mean + - SE over trials; n~10 trials per condition). (**b**) Optogenetic suppression of V1 cortex with light delivered via the Opto-Array, for the luminance discrimination task in monkey Y, yielded no substantial reaction time effects. The map shows the change in reaction time between control and illumination trials, pooling over all LED conditions. (**c**) Global effect from Opto-Array experiments, for all parameters of psychometric function, pooling over all LED conditions. We observe a reliable behavioral effect of LED illumination even at this coarse scale in the form of a substantial psychometric shift away from the ROI ($\alpha$), but not with respect to any other psychometric parameters.
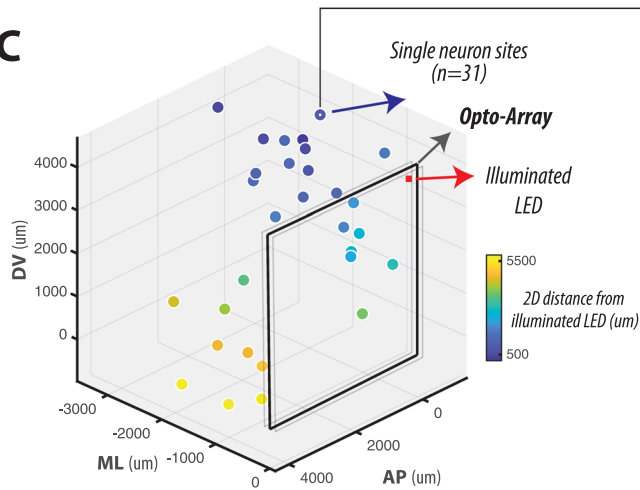
**A** Acute electrophysiology under Opto-Array in IT cortex

Stereo micro-focal x-ray

**B**

**C** Single neuron sites (n=31)

Opto-Array

Illuminated LED

2D distance from illuminated LED (um)

**D**

**Example IT neuron**

Control
LED on

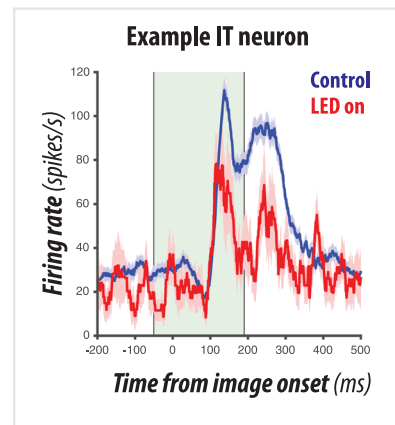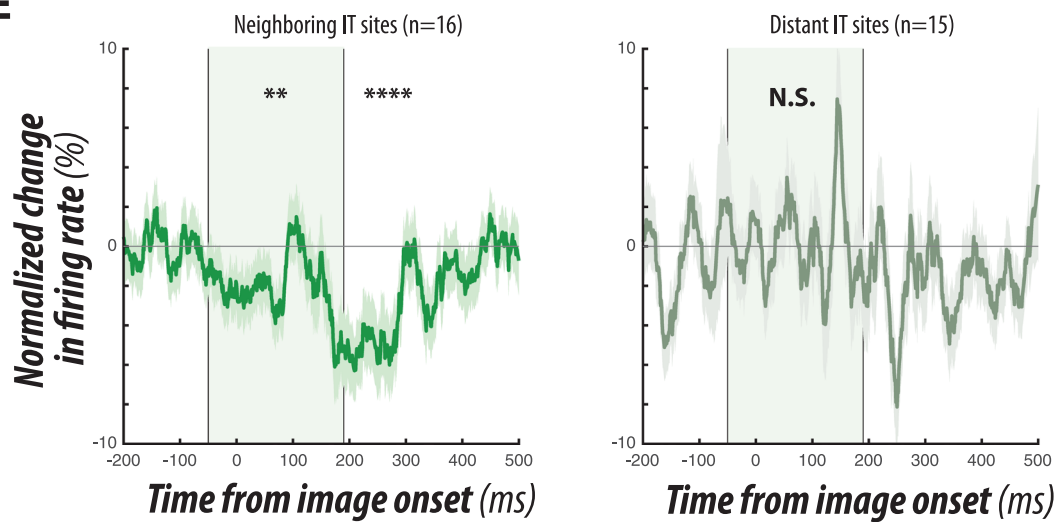**E** Neighboring IT sites (n=16) / Distant IT sites (n=15)

Extended Data Fig. 4 | See next page for caption.

**Extended Data Fig. 4 | Neural suppression using Opto-Array in IT cortex.** (**a**) (top) Coronal MRI slice highlighting the location of the implanted Opto-Array on the lateral surface of area IT (inferior temporal cortex), with the location of the recording chamber on the dorsal surface (yellow) and acutely inserted electrode driven just beneath the array (red). (bottom) High-resolution micro-focal stereo x-ray system to precisely guide our electrodes close to the array surface. (**b**) Example stereo x-ray images showing two x-ray projections of the electrode, Opto-Array, and other skull implants (here, titanium straps and mesh used for Opto-Array implant). (**c**) 3D reconstruction of recorded IT sites relative to the Opto-Array. The red square shows the illuminated LED on the Opto-Array and the colored dots show all 31 corresponding recorded IT sites. Marker color corresponds to the distance between the recorded IT and the illuminated LED, on the plane parallel to the Opto-Array. (**d**) For the example IT site shown in c, the PSTH for control and illuminated conditions are shown in blue and red. Shaded lines correspond to mean $+-$ SE, over $n > 30$ repetitions. (**e**) The percentage change in neural response between light ON and control conditions. Neural sites were split into two groups based on the 3D distance between the site location and the location of the illuminated LED ('neighboring' (left) and 'distant' (right) sites, defined as less than and greater than the median distance over all sites, respectively). Shaded lines correspond to mean $+-$ SE, over $n = 16$ multi-unit sites (left) and $n = 15$ multi-unit sites (right). The green overlays correspond to the time of LED illumination. Over all recorded neighboring neural sites, the neural suppression by light delivery was statistically significant ($p < 0.01$, one-sided exact test). Distant IT sites did not show reliable suppression ($p > 0.1$, one-sided exact test). Across all panels, asterisks are defined as: *$p < 0.05$, **$p < 0.01$, ***$p < 0.001$, ****$p < 0.0001$.
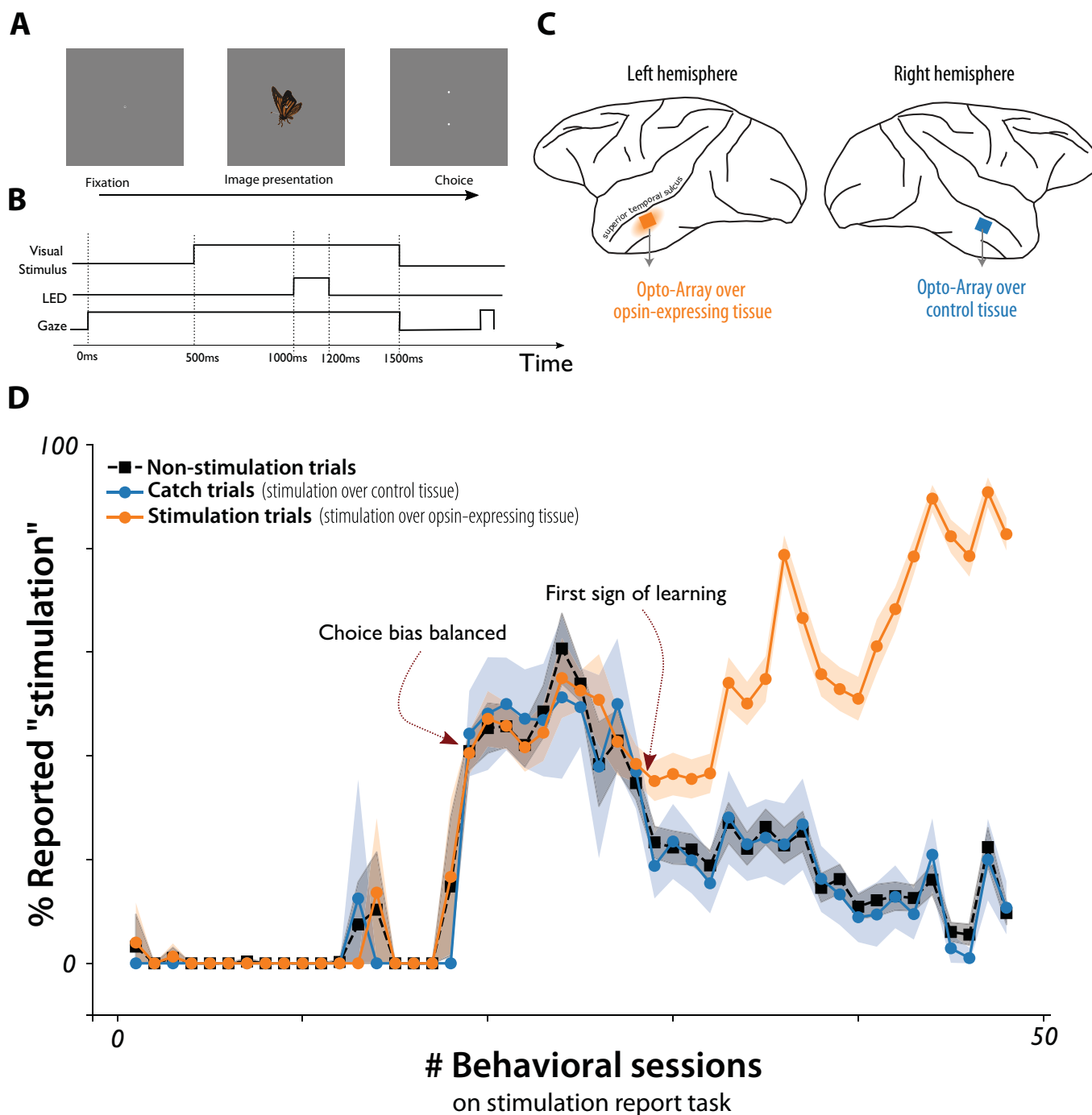
**Extended Data Fig. 5 | Behavioral deficits of optogenetic suppression in IT cortex.** (**a**) Behavioural paradigm: the animal was trained to detect optogenetic stimulation of its IT cortex. Each trial started by presenting a central fixation point and, after 500 ms of initial fixation, a visual stimulus (an image of a butterfly in this example), followed by two choice targets. This visual stimulus was presented in all conditions and was not predictive of the brain stimulation condition. (**b**) Time course of behavioral task. (**c**) We placed two arrays in similar cortical areas (IT cortex), one that had been transfected by virus, activated in the 'stimulation trials', and one that had not, activated in the 'catch trials' (10% of the trials). The three trial types were presented in random order. (**d**) The markers show the percentage of trials where the animal 'reported stimulation', as a function of training sessions separately for each trial type. The shaded areas represent 95% confidence intervals.

| | |
|---|---|
| Corresponding author(s): | Arash Afraz |
| Last updated by author(s): | May 11, 2021 |

# Reporting Summary

Nature Research wishes to improve the reproducibility of the work that we publish. This form provides structure for consistency and transparency in reporting. For further information on Nature Research policies, see our Editorial Policies and the Editorial Policy Checklist.

## Statistics

For all statistical analyses, confirm that the following items are present in the figure legend, table legend, main text, or Methods section.

| n/a | Confirmed | |
|---|---|---|
| ☐ | ☒ | The exact sample size (*n*) for each experimental group/condition, given as a discrete number and unit of measurement |
| ☐ | ☒ | A statement on whether measurements were taken from distinct samples or whether the same sample was measured repeatedly |
| ☐ | ☒ | The statistical test(s) used AND whether they are one- or two-sided<br>*Only common tests should be described solely by name; describe more complex techniques in the Methods section.* |
| ☐ | ☒ | A description of all covariates tested |
| ☐ | ☒ | A description of any assumptions or corrections, such as tests of normality and adjustment for multiple comparisons |
| ☐ | ☒ | A full description of the statistical parameters including central tendency (e.g. means) or other basic estimates (e.g. regression coefficient) AND variation (e.g. standard deviation) or associated estimates of uncertainty (e.g. confidence intervals) |
| ☐ | ☒ | For null hypothesis testing, the test statistic (e.g. *F*, *t*, *r*) with confidence intervals, effect sizes, degrees of freedom and *P* value noted<br>*Give P values as exact values whenever suitable.* |
| ☒ | ☐ | For Bayesian analysis, information on the choice of priors and Markov chain Monte Carlo settings |
| ☒ | ☐ | For hierarchical and complex designs, identification of the appropriate level for tests and full reporting of outcomes |
| ☒ | ☐ | Estimates of effect sizes (e.g. Cohen's *d*, Pearson's *r*), indicating how they were calculated |

*Our web collection on statistics for biologists contains articles on many of the points above.*

## Software and code

Policy information about availability of computer code

| Data collection | MWorks (0.9) |
|---|---|
| Data analysis | MATLAB (2019a), Python (3.6) |

For manuscripts utilizing custom algorithms or software that are central to the research but not yet described in published literature, software must be made available to editors and reviewers. We strongly encourage code deposition in a community repository (e.g. GitHub). See the Nature Research guidelines for submitting code & software for further information.

## Data

Policy information about availability of data

All manuscripts must include a data availability statement. This statement should provide the following information, where applicable:
- Accession codes, unique identifiers, or web links for publicly available datasets
- A list of figures that have associated raw data
- A description of any restrictions on data availability

Data is available on a public repository: https://github.com/RishiRajalingham/NatureMethods2021

# Field-specific reporting

Please select the one below that is the best fit for your research. If you are not sure, read the appropriate sections before making your selection.

☒ Life sciences     ☐ Behavioural & social sciences     ☐ Ecological, evolutionary & environmental sciences

For a reference copy of the document with all sections, see nature.com/documents/nr-reporting-summary-flat.pdf

# Life sciences study design

All studies must disclose on these points even when the disclosure is negative.

| | |
|---|---|
| Sample size | Given that the main behavioral experiment tests the validity of a tool, rather than make any new insights, we used n=1 monkeys for the V1 behavioral experiments. However, we have included data from two other animals, for a total of n=3 monkeys, based on the reviewers' feedback. The standard in the field is n=2 monkeys. |
| Data exclusions | We do not exclude any data pertaining to the V1 luminance discrimination experiment under Opto-Array illumination. We did not exclude any data pertaining to the IT physiology experiments showing neural suppression by LED illumination. We did not exclude any data pertaining to the IT behavioral experiments showing behavioral effects from illuminating virus-expressing IT cortex. |
| Replication | We used 4 different LED groups for the V1 luminance discrimination experiment, and successfully replicated the finding across these independent groups, as well as on data pooling over these groups. All thermal and photometric measurements were replicated across LEDs and trials, and all replications were successful. |
| Randomization | Behavioral trials were always randomly assigned to control or LED illumination conditions. |
| Blinding | Random sampling of trial conditions ensures that both the subject and the experimenter are blind to the illumination condition. |

# Reporting for specific materials, systems and methods

We require information from authors about some types of materials, experimental systems and methods used in many studies. Here, indicate whether each material, system or method listed is relevant to your study. If you are not sure if a list item applies to your research, read the appropriate section before selecting a response.

## Materials & experimental systems

| n/a | Involved in the study |
|---|---|
| ☒ | ☐ Antibodies |
| ☒ | ☐ Eukaryotic cell lines |
| ☒ | ☐ Palaeontology and archaeology |
| ☐ | ☒ Animals and other organisms |
| ☒ | ☐ Human research participants |
| ☒ | ☐ Clinical data |
| ☒ | ☐ Dual use research of concern |

## Methods

| n/a | Involved in the study |
|---|---|
| ☒ | ☐ ChIP-seq |
| ☒ | ☐ Flow cytometry |
| ☒ | ☐ MRI-based neuroimaging |

## Animals and other organisms

Policy information about studies involving animals; ARRIVE guidelines recommended for reporting animal research

| | |
|---|---|
| Laboratory animals | Macaca mulatta; all male, all adult. |
| Wild animals | no wild animals were used in the study |
| Field-collected samples | no field collected samples were used in the study |
| Ethics oversight | All procedures were performed in compliance with National Institutes of Health guidelines and the standards of the MIT Committee on Animal Care and the American Physiological Society. |

Note that full information on the approval of the study protocol must also be provided in the manuscript.